jOUrnal

J. Am. Ceram. Soc., 77 [5] 1249–55 (1994)

Fibrous Monolithic Ceramics: III, Mechanical Properties and Oxidation Behavior of the Silicon Carbide/Boron Nitride System

Suresh Baskaran[*,†] and John W. Halloran[*]

Department of Materials Science and Engineering, University of Michigan,
Ann Arbor, Michigan 48109-2136

Fibrous monolithic ceramics were fabricated in the SiC/BN system. The microstructure consists of high-aspect-ratio polycrystalline cells of SiC separated by cell boundaries of BN. The fibrous monolith with aligned cells fails non-catastrophically in flexure, with delamination cracking along the BN cell boundaries. Indentations cause controlled damage on the surface, but no strength-degrading flaws. The flexural strength is in the range 300–375 MPa, and the estimated shear strength is ≈14 MPa. The SiC/BN fibrous monoliths also show excellent resistance to high-temperature oxidation in air. Noncatastrophic fracture behavior is observed at room temperature after heat treatments between 1200° and 1500°C. The SiC cells on the surface are oxidized to form a protective silicate scale, which prevents deterioration of the BN cell boundaries.

I. Introduction

THE incorporation of high-strength ceramic fibers in ceramic matrices has led to a new generation of advanced composites with high toughness and graceful failure characteristics.[1,2] Fiber-reinforced ceramic matrix composites are candidate materials for many lightweight, high-temperature structural applications such as gas turbine engine components. However, these materials have found only limited use because of their high cost. Composites use expensive fibers, and must be fabricated using costly processing methods such as coatings by chemical vapor deposition and, in some cases, matrix formation by chemical vapor infiltration. A monolithic ceramic material fabricated with inexpensive powders and showing noncatastrophic fracture behavior would prove to be more useful. Clegg *et al.*[3] demonstrated this concept with tough SiC/graphite tape-cast laminates in which the graphite interlayers delaminated during flexural failure. Similarly, SiC-based ceramics fabricated from powders by the "fibrous monolith" approach[4] have shown useful mechanical properties.[5,6] These new materials have commercial potential because of their damage-tolerant mechanical behavior combined with low cost.

The "fibrous monolith" microstructure consists of high-aspect-ratio polycrystalline cells of a primary phase separated by thin cell boundaries of a second phase.[5] There are no reinforcing fibers. The cells are polycrystalline regions (e.g., SiC) that are remnants of "green" powder-loaded polymer fibers. A coating applied on the green fiber forms the cell boundary, which can be any thermodynamically compatible second phase designed to enhance the fracture resistance of the material. When the cell boundary is graphite, there is preferred crack propagation along the cell boundaries. The fibrous monolith fails noncatastrophically in flexure and is flaw-tolerant and notch-insensitive.[6]

SiC/graphite fibrous monoliths have limited applications because of oxidation of the graphite cell boundaries at high temperatures in air. Thermogravimetric analysis of SiC/graphite fibrous monoliths has shown that weight loss due to oxidation of cell boundaries begins at ≈250°C and is complete after 1 h at 700°C.[7] An alternative weak cell boundary material with better oxidation resistance is hexagonal (α) boron nitride, which is similar in structure to graphite. High-performance fiber-reinforced composites have been fabricated with CVD coatings of BN on fibers.[8–10] The weak BN interfacial layers between fibers and matrix result in debonding and fiber pullout, giving rise to useful fracture behavior. In this paper, processing and mechanical properties of SiC/BN fibrous monoliths are described. Fracture behavior is compared with SiC monolith and SiC/graphite fibrous monolith.[6,11] The effect of oxidation is evaluated by microstructural analysis and room-temperature flexural tests after high-temperature treatments in air.

II. Experimental Procedure

Suspensions of SiC powder (B-10, β-SiC powder, H. C. Starck, New York) in an ethyl methacrylate (EMA)/methyl ethyl ketone (MEK) solution (B7/MEK Acryloid, 30 wt% solution, Rohm and Haas, Philadelphia, PA) were ball-milled, and then concentrated by evaporation of the MEK. The concentrated "dopes" were extruded to form soft "green fibers" by dry-spinning into a hot-air column maintained at 100°C. Yttria (Johnson Matthey, Ward Hill, MA) and alumina (RC-HP DBM, Malakoff Industries, Malakoff, TX) were used as sintering aids. The weight ratio of $SiC:Y_2O_3:Al_2O_3$ was 90:4:6. The volume ratio of ceramic powder to ethyl methacrylate polymer in the dry fiber was 55:45. Green fibers typically had a "dog-bone" cross section,[5] with an area-equivalent circular diameter of ≈150–200 μm.

The green fibers were run through a coating slurry of BN(+ Al_2O_3)[‡] immediately after extrusion. Boron nitride was present as 1–10-μm-wide platelets in suspension. The coated fibers were loaded in a 52 mm × 26 mm graphite die using one of two fiber architectures: either aligned fibers using ≈51-mm lengths or finely chopped, randomly oriented fiber segments. To simply evaluate the fracture behavior, both die filling techniques were tested. To study the effect of oxidation treatments, only aligned fiber billets were used. The chopped fiber die-filling method was evaluated because it was relatively easy.

The green fibers were pressed at ≈80°C, using 5-MPa pressure. This softens the polymer and consolidates the fibers into a dense monolithic billet with 45 vol% polymer. After removal of the polymer binder between 200°C and 600°C in an actively pumped vacuum, the billet was hot-pressed at 1900°C in argon

for 1 h, using 25-MPa ram pressure. Hot-pressed billets were 4.0–4.5 mm in thickness.

Most hot-pressed billets were machined into bar specimens 3 mm thick, 4 mm wide, and 48 mm long. Three bar specimens from an aligned fiber billet were machined down to 1-mm thickness. The 3-mm-thick samples provided a span-to-depth ratio of 3.33, which caused samples to fail by midplane shear cracking.[6,12] The 1-mm-thick samples were used to evaluate the true flexural strength of the material at high ($\approx$9) span-to-depth ratio. All bars were machined and chamfered with a 1000-grit resin-bonded diamond wheel, with the grinding direction parallel to the length of the specimen. The tension side was normal to the pressing direction. In some cases, the side surfaces of samples were polished prior to testing. Flexural strength was measured using a fully articulated four-point bend fixture with a 20-mm inner span and a 40-mm outer span at a crosshead speed of 0.05 mm/min. Stress values were calculated from elastic beam equations.

The density of the bars was measured by the Archimedes method. Young's modulus was measured on bar specimens by the flexural resonance method[13,14] (Grindo-Sonic, J. W. Lemmens, St. Louis, MO). In this technique, the bar is set in resonance, and the frequency is measured with a contact probe. Damage and cracking from Vickers indentations were studied using a Zwick (E. Windsor, CT) indenter. An indentation load of 5 kg ($\approx$50 N) was used with 30-s residence time.

Machined bar specimens of 3-mm thickness were heat-treated in air at high temperatures. Bars were held for 10 h between 1200° and 1500°C. Some bars were also held at 1400°C for 10, 50, and 250 h. Heating and cooling rates were 15°C/min between $\approx$500°C and the heat-treatment temperature. Heat-treated bars were tested in flexure. The 3-mm-thick specimens were used to study the effect of oxidation on the material's shear characteristics which are responsible for the noncatastrophic fracture behavior.

After testing, all heat-treated bars were inspected, using optical and scanning electron microscopy. Bars invariably shear cracked on only one-half of the specimen. Cross sections $\approx$5 mm from the undamaged end were polished and then studied by optical microscopy. Elemental analysis was done on polished sections with an electron microprobe, using X-ray wavelength dispersive spectrometry and appropriate standards.

III. Results and Discussion

(1) Microstructure, Elastic Modulus, and Indentation Behavior

The microstructure of SiC/BN fibrous monoliths with aligned fibers is shown in Fig. 1. Flattened SiC cells 50–100 μm thick and 150–200 μm wide are separated by cell boundaries a few micrometers to $\approx$25 μm in thickness. The cell sections visible in the micrographs of Figs. 1(A) and (C) vary in length from about 200 μm to several millimeters in the long direction of the billet. Although long green fibers are placed in the die, the forming procedure can result in finite cell lengths. Green fibers can fracture or bend and also may not lie perfectly normal to the pressing direction or perfectly parallel to the long die wall. Only short cell segments are visible in the micrographs, but individual cells could actually have continuity and extend for longer distances (approximately a few centimeters) up to a maximum of 5.2 cm.

The microstructure of a chopped fiber monolith is shown in Fig. 2. Here the cell cross sections on surfaces parallel to the pressing direction are quite small. Cell lengths vary from 200 to 600 μm. Viewed in the pressing direction, the sample consists of randomly oriented cells several hundred micrometers long and about 200 μm wide.

The volume fraction of the cell boundary was determined to be $\approx$23 vol% from point counts on optical micrographs of cell cross sections. The analyzed area encompassed about 300 cells. The 23 vol% cell boundary in SiC/BN is considerably more

than the 8 vol% cell boundary in SiC/graphite.[6] This reflects the differences in coating thickness from the commercial BN slurry used in this study and the diluted Aquadag (Acheson Colloid, Port Huron, MI) graphite slurry used to fabricate SiC/graphite.[6]

The SiC cell microstructure is shown in Fig. 3. The backscattered electron image from the electron microprobe shows elongated grains of SiC with the yttria–alumina intergranular phase in bright contrast. The cell phase determined by X-ray diffraction was predominantly β-SiC, with 10–20 vol% hexagonal SiC polytypes.

The density of the SiC/BN fibrous monolith was 2.99 g/cm^3. The samples did not imbibe water. The density of the cells is inferred by comparison to the SiC monolith (i.e., hot-pressed SiC with yttria and alumina), which was 3.20 g/cm^3. By combining this information, the cell boundaries are estimated to be $\approx$96 vol% BN($+ Al_2O_3$) and $\approx$4 vol% porosity.

For aligned fibrous monoliths, Young's modulus measured on two bar specimens was 341–342 GPa. Single-phase polycrystalline SiC densified with small additions of B and C has modulus ranging from 410 to 440 GPa.[15] The lower modulus compared to SiC reflects the contributions from $\approx$8 vol% yttria–alumina within cells and the high volume fraction of the lower-modulus BN cell boundary phase. The modulus of hot-pressed single-phase hexagonal BN is in the range 35–72 GPa,[16] and there is $\approx$23 vol% of this cell boundary. Literature values of Young's modulus values for SiC/BN particulate composites with 20 vol% BN are in the range 260–320 GPa.[17] The elastic modulus of SiC/graphite fibrous monolith measured by the same technique was slightly higher at 355–360 GPa, presumably due to lower ($\approx$8 vol%) cell boundary content.[11] Combined with the low density, the modulus of the aligned fiber SiC/BN makes this material useful in applications requiring high specific modulus.

For the chopped-fiber layout, the modulus was significantly lower (275 GPa). The lower modulus can arise from both cell geometry considerations and BN texture within the cell boundaries. With the chopped-fiber layout, many cells lie at orientations almost perpendicular to the bar axis. A higher volume fraction of the BN cell boundaries lies in series with the SiC in the axial direction of the bar, resulting in lower stiffness. Furthermore, the coating process and the compaction could result in some alignment of cell boundary platelets along cell axes. In the randomly oriented cell geometry, where cells can lie normal to the bar axis, a significant fraction of BN platelets at the cell boundaries could be oriented with their weak c-axis direction along the bar axis. This could also result in lower elastic modulus.

From scanning electron microscopy of polished cross sections, it was difficult to determine whether platelets had preferred orientation. But X-ray diffraction of an aligned fiber monolith showed evidence of texture in the BN cell boundaries. The integrated intensity ratios of $(002)_{BN}$ to $(001)_{b-SiC}$ were 1:1.2, 1:4.2 and 1:15 from the sample cross sections shown in Figs. 1(A), (C), and (B), respectively. Other BN peaks were too weak to give useful information. The integrated intensity ratios indicate that BN platelets were mostly aligned with their c-axes in the hot-pressing direction. The preferred orientation of the lubricious BN platelets due to hot-pressing should result in low shear strength on planes normal to the pressing direction. From the moderate intensity of the $(002)_{BN}$ from the side of the specimen (cross section in Fig. 1(C)), there also appears to be some alignment of the BN platelets with their c-axes normal to the pressing direction and the cell axes. This alignment must result from slurry application on the green fibers.

Surface damage from a Vickers indentation is shown in Fig. 4. The section of a chopped fiber pellet parallel to the pressing direction was indented. Indentation causes cells to spall or crack, with the soft BN being extruded out from the cell boundaries. Unlike classically brittle materials, long radial cracks do not form upon indentation. So, just as in SiC/graphite,[6] strength would be unaffected by point contact damage.
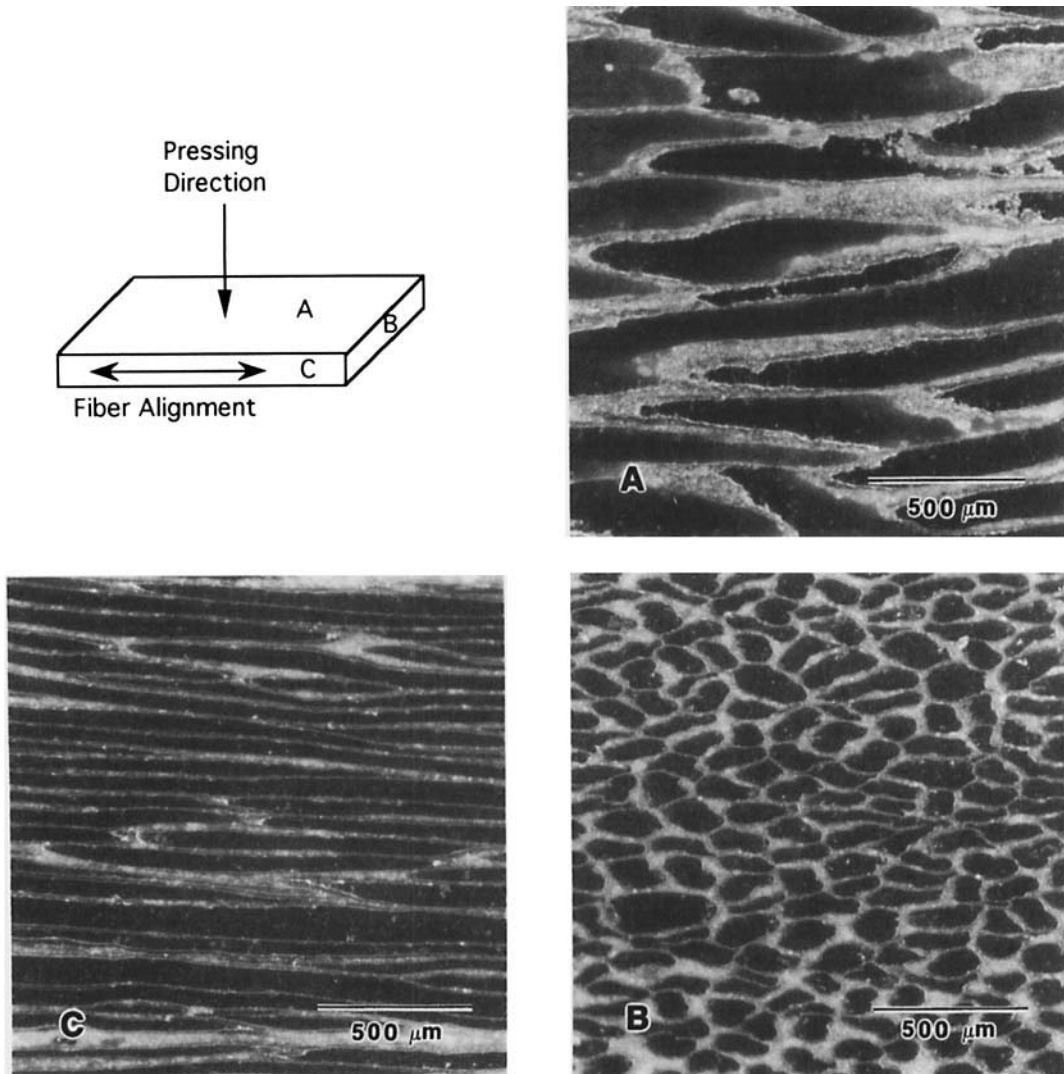
Fig. 1. Optical micrographs of a SiC/BN fibrous monolith prepared with aligned green fibers showing polycrystalline SiC cells (dark) and BN cell boundaries (light).
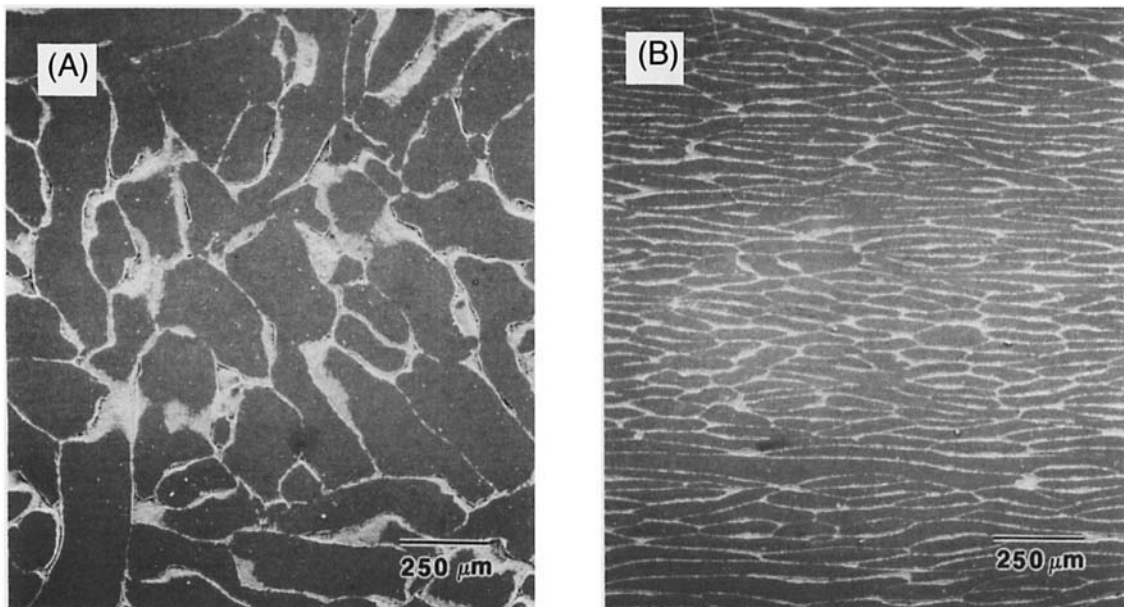
Fig. 2. SEM micrographs of polished surfaces of a SiC/BN fibrous monolith prepared with finely chopped, randomly oriented fibers (A) viewed in the hot-pressing direction and (B) viewed normal to the hot-pressing direction.
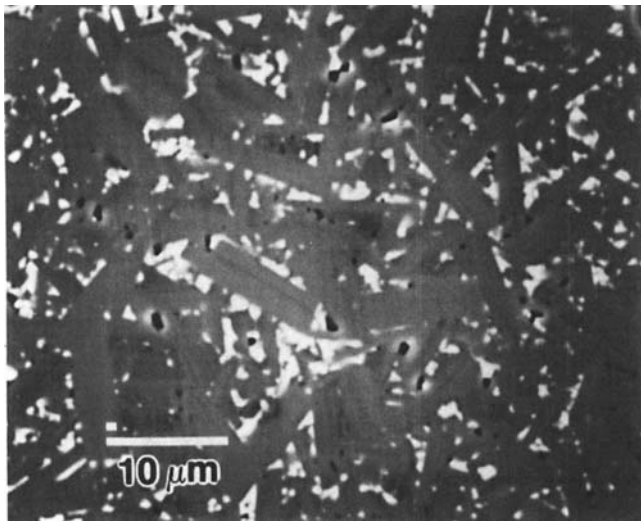
Fig. 3. Backscattered electron image of a SiC cell showing elongated grains of SiC (gray), and the yttria–alumina intergranular phase (white).
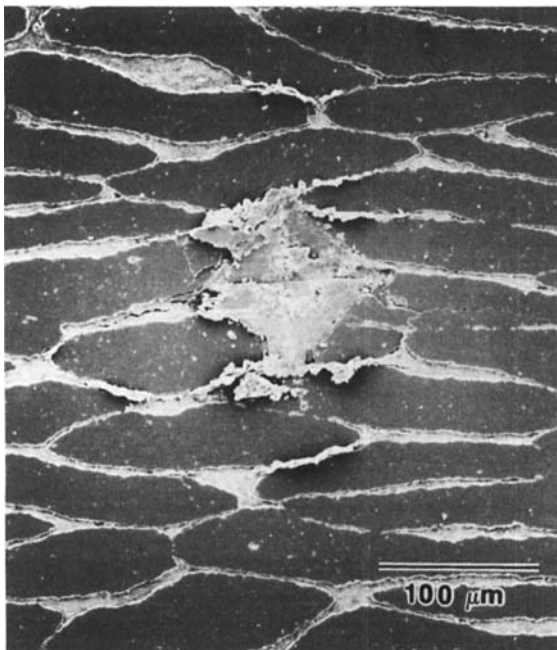

Fig. 4. SEM micrograph showing indentation fracture in a SiC/BN fibrous monolith (load = 50 N). Indented surface was parallel to the hot-pressing direction. Note extrusion of cell boundary material and absence of long radial cracks.

(2) Flexural Strength and Fracture Behavior

Load–deflection curves for two sample geometries of aligned-fiber SiC/BN are compared with data for a SiC monolith[11] in Fig. 5. The applied stress value is meaningful until the first load drop in each of the samples. The SiC monolith shows high strength but brittle fracture behavior. The fibrous monoliths for both span-to-depth ratios display noncatastrophic fracture behavior, with significant load-retaining capability after fracture commences. The lower modulus of the fibrous monolith is apparent from the lower slope of the 3-mm-thick SiC/BN specimen compared to SiC.

The strength values and modes of fracture were very similar to the SiC/graphite.[6] For thin specimens, fracture initiated from the tension side, and the sample then proceeded to delaminate like wood. The flexural strength values measured at this high
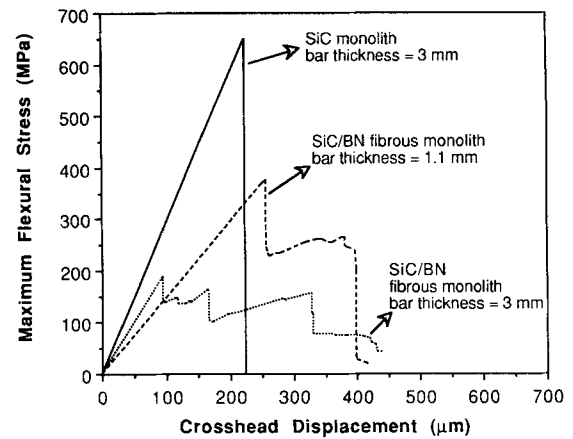

Fig. 5. Flexural strength behavior of aligned-fiber SiC/BN compared to monolithic SiC. Load–deflection traces for the fibrous monolith at two different span-to-depth ratios are shown.

span-to-depth ratio were in the range 300–375 MPa. For thick specimens, the samples shear-cracked starting at the midplane of the bar specimens between an inner and an outer loading point, where applied shear stresses are highest. The apparent strength of 186 MPa is not meaningful, since failure begins when the applied $\tau_{midplane}$ reaches the shear strength of the material. The interlaminar shear strength estimated from the thick specimens using elastic beam equations[6,12] was 14.1 MPa. The side surface after the test for a 3-mm-thick specimen is shown in Fig. 6. Extensive delamination cracking occurs along the length of the bar specimen. An apparent work-of-fracture measured from the area under the load–displacement curve and the specimen cross-sectional area was 2430 J/m^2.

The load–deflection behavior for a chopped-fiber bar specimen in flexure is presented in Fig. 7(A). The strength is 128 MPa, almost identical to the strength of SiC/graphite with similar cell architecture.[6] The side surface of the specimen after testing is shown in Fig. 7(B). Fracture initiates at the weak cell boundaries normal to the applied stress on the tension side. The shear characteristics of the material cause the crack to deflect towards the bar axis and propagate along the weak cell boundaries. The specimen does not fall apart after the test, but has almost no load-bearing capability.

From the cell architectures studied, it appears that, with suitable fiber lay-up methods, SiC/BN fibrous monoliths can be fabricated with sufficient strength and tough fracture behavior. Earlier work with SiC/graphite[11] has shown that the off-axis strength in aligned fibrous monoliths is low ($\approx$70 MPa), but
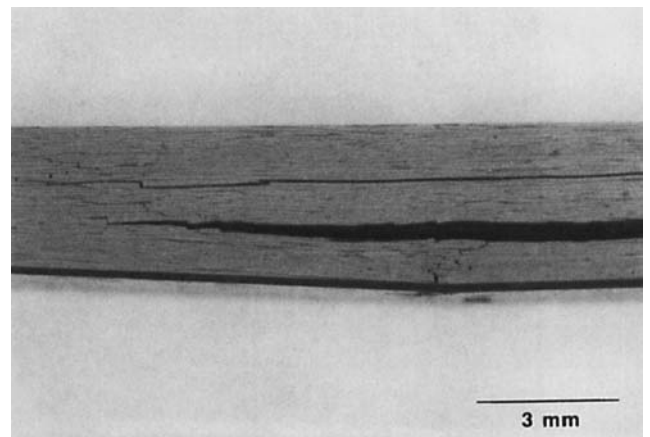

Fig. 6. Side surface of SiC/BN bend specimen after test showing delamination cracking (optical micrograph).
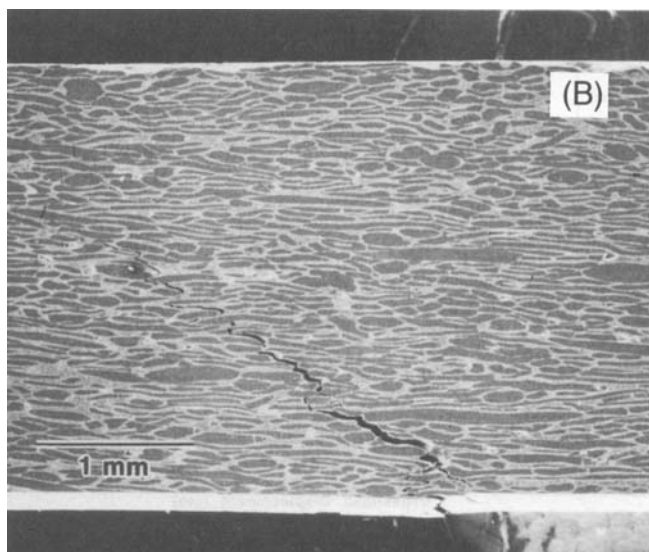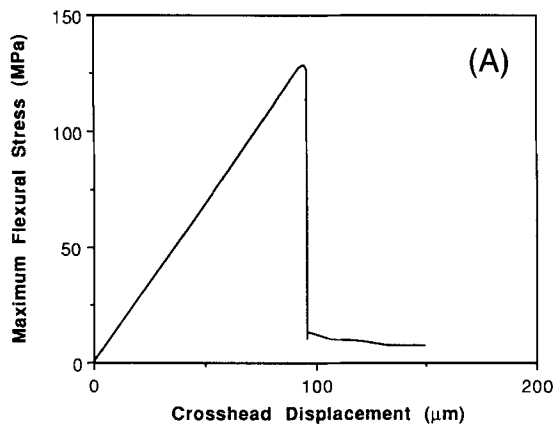
Fig. 7. (A) Flexural strength behavior of chopped-fiber SiC/BN. (B) SEM micrograph of the side surface of the specimen after test.

a 0°/90° cross-ply structure has strength ≈150 MPa. Other microstructural arrangements such as woven fabrics of SiC/BN may have a combination of tensile and shear strengths that meets design requirements of some structural components.

(3) Effect of Oxidation

The room-temperature strength behavior of oxidized bars after 10-h heat treatments at 1200° to 1500°C in air is shown in Fig. 8. Noncatastrophic fracture behavior is observed even in samples heat-treated to 1500°C. All samples were glazed after heat treatment. The bar specimens' thickness and width had increased about 3%–4%. The high temperature (1400° and 1500°C) heat treatments resulted in substantial bubble formation, with gas entrapment and foaminess in the scale. In the sample held at 1500°C, the scale had foamed up a few millimeters, presumably because of lower viscosity of the scale at the high temperature. For this specimen, the foam was scraped off before testing. In Fig. 8, the apparent strengths are again not meaningful and do not reflect the true flexural strength of the materials. For all samples, failure initiated by midplane shear cracking, followed by extensive damage primarily below the inner loading point. The oxidation treatment had apparently not affected the shear properties (i.e., not affected the bulk of the BN cell boundaries) significantly. Then the bar specimen shear cracked between an inner and outer loading point, which chipped off part of the scale, as shown in Fig. 9.
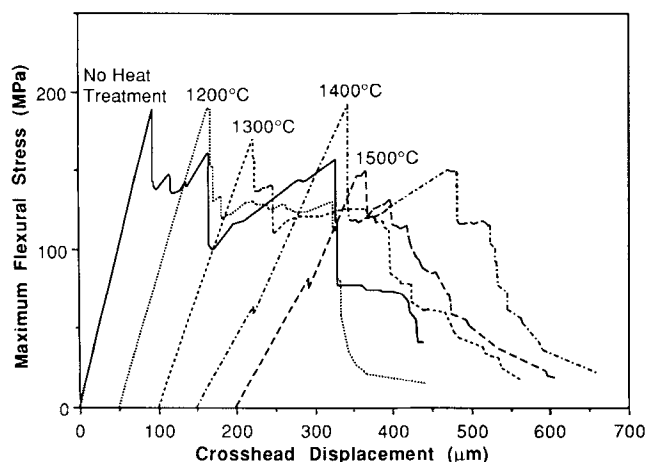
The room-temperature load deflection behavior of bar specimens heat-treated at 1400° for 10, 50, and 250 h is shown in Fig. 10. Here again, all samples failed by shear delamination along the cell boundaries. Noncatastrophic fracture behavior was recorded even after 250 h (>10 days) at 1400°C. The bar that had undergone the long 250-h heat treatment was covered with a foamy, translucent scale. The side surface of this bar in Fig. 11 shows delamination cracking and damage in the section below the inner loading point. The fibrous structure is visible in regions where the scale has come off.

Table I lists the room-temperature flexure properties for all the SiC/BN samples after heat treatment. Interlaminar shear strengths calculated from the maximum flexural stress are generally low after all the heat treatments. The long 1400°C hold results in some increase in the shear strength to 18 MPa. Apparent work-of-fracture values are also high for all the specimens.

The polished section of a bar specimen after 1400°C/250 h is compared with an untreated sample in Fig. 12. The optical micrographs show the chamfered corners of the bar section. The scale on the heat-treated sample is 25–50 μm thick on average, and >100 μm thick in some areas. There was no measurable
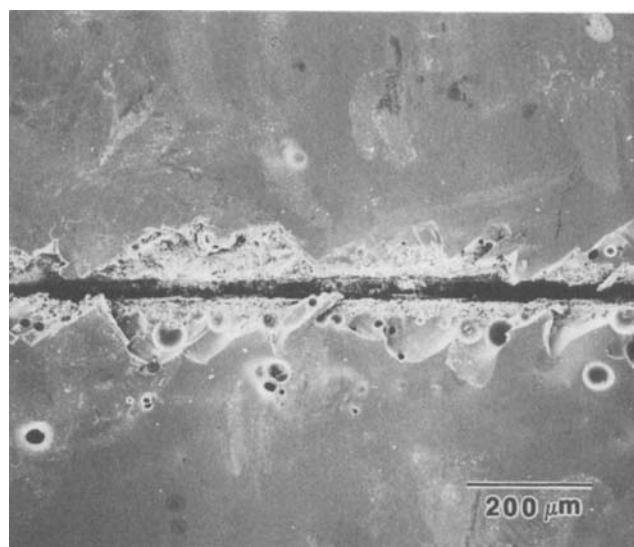

Fig. 8. Room-temperature strength behavior of aligned-fiber SiC/BN after 10-h heat treatments in air at high temperatures.

Fig. 9. SEM micrograph showing side surface of heat-treated (1400°C/10 h) SiC/BN specimen after bend test.
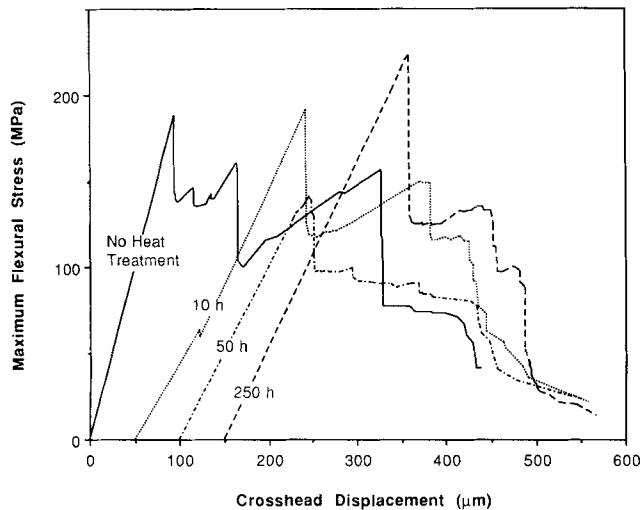
Fig. 10. Room-temperature strength behavior of aligned-fiber SiC/BN heat-treated at 1400°C in air for various times.

Table I. Room-Temperature Properties of Aligned-Fiber SiC/BN from Flexure Tests

Heat treatment	σ_{max} (MPa)	$\tau_{failure}$ (MPa)	Apparent work-of-fracture (J/m²)
None	186	14.1	2430
1200°C (10 h)	189	14.7	1770
1300°C (10 h)	171	13.5	2130
1400°C (10 h)	192	15.6	2210
1500°C (10 h)	146	11.6	1480
1400°C (50 h)	141	11.3	1800
1400°C (250 h)	223	18.0	2230

change in the cell and cell boundary dimensions. There was also no evidence of degradation or reactions in the cell boundaries or cells in the interior of the sample. This is consistent with retention of low-shear-strength BN cell boundaries and noncatastrophic fracture behavior even after 10 d at 1400°C.

A backscattered electron image of a polished section of heat-treated SiC/BN is shown in Fig. 13. The micrograph shows the
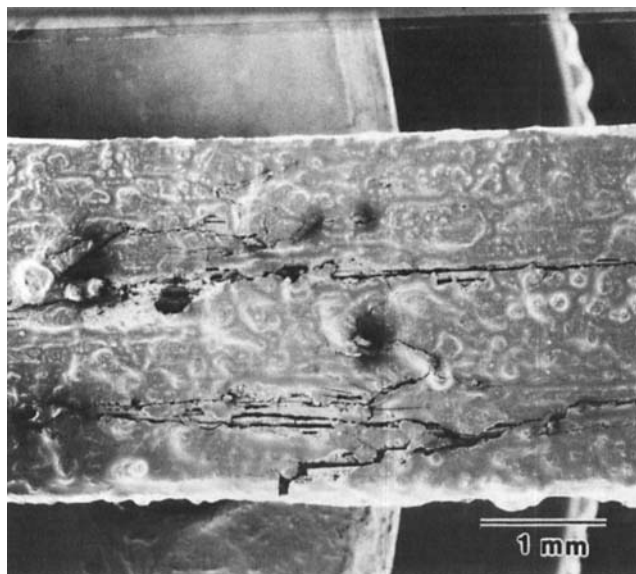

Fig. 11. SEM micrograph showing side surface of heat-treated (1400°C/250 h) SiC/BN specimen after bend test.

scale appearing in bright contrast. The scale contains faceted inclusions. The SiC cell in the interior, as in Fig. 3, shows bright Y- and Al-containing intergranular phases. Elemental microanalysis was done on the different phases in many areas of this sample, as well as on unoxidized samples. The bright scale contained yttrium, aluminum, silicon, and oxygen. The inclusion was a crystalline form of silica, most likely cristobalite.[18] There was no evidence of an oxidation product of BN extending into the BN-rich cell boundary. It was not possible to determine whether boron was present in the scale, since our spectrometer could not detect boron in this sample. A wavelength spectrometer scan of the emissions from the scale did not show the characteristic peak for nitrogen, which indicated that there was no dissolved N in the glass. The compositions of the cell phase were the same in the unoxidized and heat-treated samples. Some pieces of monolithic SiC (with the same yttria–alumina additions) were also heat-treated for comparison. Similar oxide scale formation was observed in these samples, with identical elemental compositions.

From the microstructural observations and elemental analysis, it is evident that the SiC cells on the surface are oxidized to form a protective layer of Y–Al-containing silicate scale with SiO_2 inclusions. BN appears to be unoxidized beneath this scale even after long-term exposure at 1400°C. The stability of BN in this environment can be explained in terms of the equilibrium partial pressures of oxygen expected at SiC/SiO_2 and BN/B_2O_3 interfaces at 1400°C. The oxidation of SiC is assumed to be controlled both by diffusion and interface reaction, as suggested by Luthra.[18] The most probable reaction for the oxidation of SiC cells is

$$SiC + \tfrac{3}{2}O_2 \rightarrow SiO_2 + CO$$
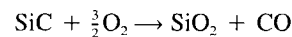
From free energies of formation,[19] ΔG for the above reaction can be calculated. With this information, and assuming 1 bar (≈ 1 atm) pressure of CO at the interface, the equilibrium P_{O_2} at the SiC/SiO_2 interface has been estimated to be $\approx 7 \times 10^{-17}$ atm.

The oxygen partial pressure required for BN oxidation can also be calculated from the free-energy change of the reaction

$$2BN + \tfrac{3}{2}O_2 \rightarrow B_2O_3 + N_2$$
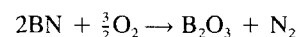
The nitrogen partial pressure beneath the scale can be assumed to be 1 bar. The equilibrium P_{O_2} at a hypothetical BN/B_2O_3 interface is then calculated to be 1.5×10^{-14}. This value of oxygen partial pressure is ≈ 150 times the equilibrium P_{O_2} at SiC/SiO_2 interfaces. The calculated value for the P_{O_2} at the SiC/SiO_2 interface is not expected to be significantly different when the oxidation product is a Y–Al–Si–O scale containing SiO_2 inclusions. The low equilibrium P_{O_2} associated with SiC oxidation establishes the oxygen partial pressure beneath the scale; this pressure is then too low for BN oxidation at 1200°–1500°C. The material retains low interlaminar shear strength BN cell boundaries after heat treatment, resulting in graceful failure behavior at room temperature. Further work on oxidation and high-temperature flexure properties is under way and will be reported in subsequent papers.

IV. Conclusion

SiC-based fibrous monoliths with weak cell boundaries of BN show potentially useful mechanical properties at room temperature. Noncatastrophic fracture behavior with significant load-bearing capability is observed in SiC/BN with aligned green fibers. As in SiC/graphite, delamination cracking of the BN cell boundaries occurs during failure. Young's modulus of SiC/BN with aligned fibers is ≈ 340 GPa. Flexural strength is in the range 300–375 MPa, and interlaminar shear strength on planes normal to the pressing direction is ≈ 14 MPa. The low shear strength should render the material notch-insensitive under flexural loading conditions. Delamination cracks initiated
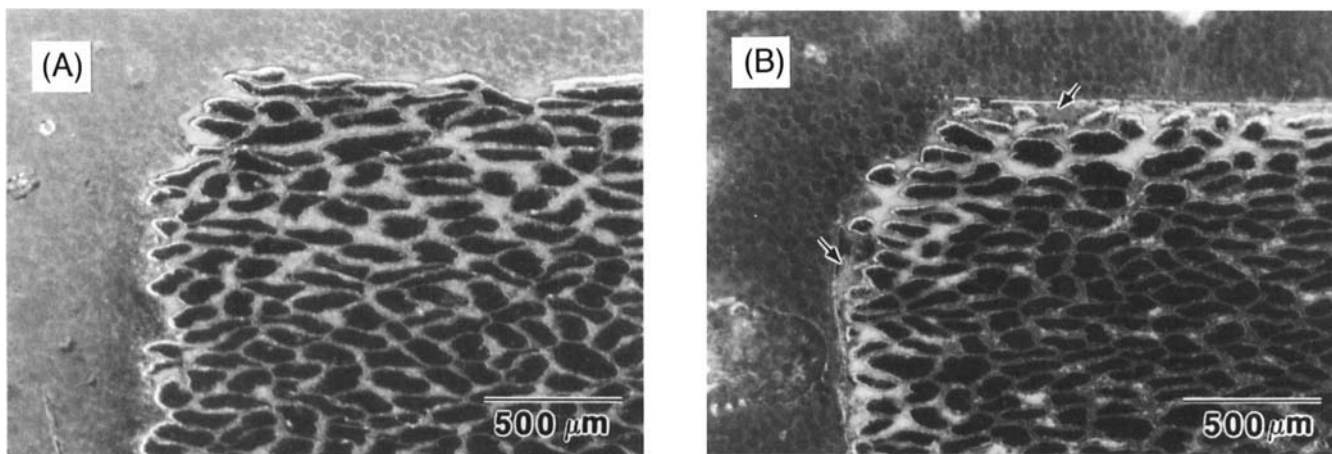
Fig. 12. Optical micrographs comparing polished cross sections of (A) unoxidized SiC/BN and (B) SiC/BN after 1400°C/250 h. Scale is indicated by arrows.
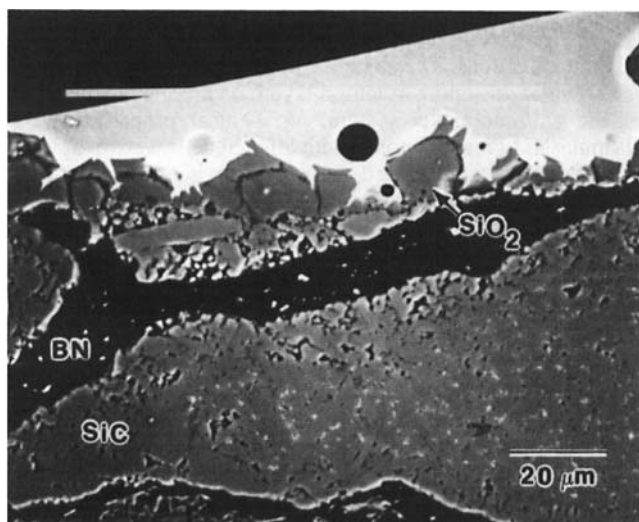

Fig. 13. Backscattered electron image of a polished section of SiC/BN heat-treated to 1400°C/250 h. The edge of the sample is shown with the various phases labeled.

from notch tips will cause the load to rise even after cracking has begun.[6]

The SiC/BN system also shows potential for use in oxidizing environments at high temperatures. The low-shear-strength BN cell boundaries are retained even after heat treatment at 1400°C for 10 days in air. The oxidation of SiC cells on the surface forms a protective silicate layer preventing the oxidation of sub-surface BN cell boundaries. Shear cracking and noncatastrophic failure is observed in room-temperature flexure tests after heat treatments in air between 1200° and 1500°C. Further studies on these materials will include evaluation of high-temperature mechanical properties, and microstructural refinement of the cell and cell boundary phases to optimize properties.

References

[1]K. M. Prewo and J. J. Brennan, "High Strength Silicon Carbide Fiber-Reinforced Glass–Matrix Composites," *J. Mater. Sci.*, **15**, 463–68 (1980).
[2]K. M. Prewo, "Fiber-Reinforced Ceramics: New Opportunities for Composite Applications," *Am. Ceram. Soc. Bull.*, **68** [2] 395–400 (1989).
[3]W. J. Clegg, K. Kendall, N. McN. Alford, T. W. Button, and J. D. Birchall, "A Simple Way to Make Tough Ceramics," *Nature*, **347**, 455–57 (1990).
[4]W. S. Coblenz, "Fibrous Monolithic Ceramic and Method for Production," U.S. Pat. No. 4772524, September 20, 1988.
[5]S. Baskaran, S. D. Nunn, D. Popovic, and J. W. Halloran, "Fibrous Monolithic Ceramics: I, Fabrication, Microstructure, and Indentation Behavior," *J. Am. Ceram. Soc.*, **76** [9] 2209–16 (1993).
[6]S. Baskaran and J. W. Halloran, "Fibrous Monolithic Ceramics: II, Flexural Strength and Fracture Behavior of the Silicon Carbide/Graphite System," *J. Am. Ceram. Soc.*, **76** [9] 2217–24 (1993).
[7]C. Arens, "Oxidation of Fibrous Monolithic Ceramics"; M.S. thesis in progress, University of Michigan, Ann Arbor, MI, unpublished work.
[8]R. N. Singh and M. K. Brun, "Effect of Boron Nitride Coating on Fiber–Matrix Interactions," *Ceram. Eng. Sci. Proc.*, **8** [7–8] 636–43 (1987).
[9]R. N. Singh and A. R. Gaddipati, "Mechanical Properties of a Uniaxially Reinforced Mullite–Silicon Carbide Composite," *J. Am. Ceram. Soc.*, **71** [2] C-100–C-103 (1988).
[10]J. J. Brennan, "Glass and Glass-Ceramic Matrix Composites"; presented at the 95th Annual Meeting of the American Ceramic Society, Cincinnati, OH, April 1993 (Paper No. SII-81-93).
[11]S. Baskaran and J. W. Halloran, "SiC-based Fibrous Monolithic Ceramics," *Ceram. Eng. Sci. Proc.*, in press.
[12]D. B. Marshall and A. G. Evans, "Failure Mechanisms in Ceramic-Fiber/Ceramic-Matrix Composites," *J. Am. Ceram. Soc.*, **68** [5] 225–31 (1985).
[13]E. Schreiber, O. L. Anderson, and N. Soga, *Elastic Constants and Their Measurement*; Ch. 4. McGraw-Hill, New York, 1973.
[14]S. Spinner and W. E. Tefft, "A Method for Determining Mechanical Resonance Frequencies and for Calculating Elastic Moduli from these Frequencies," *Proc. Am. Soc. Test. Mater.*, **61**, 1229 (1961).
[15]S. J. Schneider (Ed.), Engineering Materials Handbook, Vol. 4, *Ceramics and Glass*, Sect. II, Properties of Carbides. ASM International, Metals Park, OH, 1991.
[16]A. Lipp, K. A. Schwetz, and K. Harold, "Hexagonal Boron Nitride: Fabrication, Properties and Applications," *J. Eur. Ceram. Soc.*, **5**, 3–9 (1989).
[17]R. Ruh, A. Zangvil, and R. R. Wills, "Phase and Property Studies of SiC/BN Composites," *Adv. Ceram. Mater.*, **3** [4] 411–15 (1988).
[18]K. L. Luthra, "Some New Perspectives on Oxidation of Silicon Carbide and Silicon Nitride," *J. Am. Ceram. Soc.*, **74** [5] 1095–103 (1991).
[19]D. R. Stull and H. Prophet (Eds.), *JANAF Thermochemical Tables*, 2nd ed. National Bureau of Standards, Washington, DC, 1971.   □